Applied Catalysis B: Environmental 223 (2018) 234–241

Contents lists available at ScienceDirect

Applied Catalysis B: Environmental

journal homepage: www.elsevier.com/locate/apcatb

# [Fe($C_5Ar_5$)$(CO)_2$Br] complexes as hydrogenase mimics for the catalytic hydrogen evolution reaction

E.B. Hemming[a], B. Chan[b], P. Turner[c], L. Corcilius[a], J.R. Price[c], M.G. Gardiner[d], A.F. Masters[a], T. Maschmeyer[a,*]

[a] Laboratory of Advanced Catalysis for Sustainability, School of Chemistry, University of Sydney, NSW, 2006, Australia
[b] Graduate School of Engineering, Nagasaki University, Bunkyo 1-14, Nagasaki 852-8521, Japan
[c] School of Chemistry, University of Sydney, NSW, 2006, Australia
[d] School of Physical Sciences (Chemistry), University of Tasmania, Tas, 7005, Australia

ARTICLE INFO

*Article history:*
Received 14 October 2016
Received in revised form 10 April 2017
Accepted 20 April 2017
Available online 23 April 2017

*Keywords:*
Hydrogenase mimics
Hydrogen evolution catalysts
Electrochemistry
Iron-based catalysts

ABSTRACT

A new iron-based hydrogenase mimic, [Fe($C_5$($p$-$C_6H_4Br)_5$)$(CO)_2$Br], was synthesised and characterised using X-ray crystallography. Two analogous catalytic precursors, [Fe($C_5Ar_5$)$(CO)_2$Br] (Ar = $C_6H_5$; $p$-$C_6H_4Br$), were also analysed electrochemically in order to investigate how bulkier and more electron withdrawing $C_5Ar_5$ ligands affect the catalytic generation of hydrogen from trichloroacetic acid. Compared to previously reported iron-based cyclopentadienyl analogues, these complexes were found to have smaller overpotentials and larger turnover numbers. The [Fe($C_5$($p$-$C_6H_4Br)_5$)$(CO)_2$Br] complex was found to be the most efficient of the two catalytic precursors with a turnover number of 25, an overpotential of around 310 mV and a faster rate of reaction compared to [Fe($C_5Ph_5$)$(CO)_2$Br].



## 1. Introduction

Modern society is heavily reliant on a steady supply of energy in all aspects of daily life. Currently 82% of energy consumed globally is supplied by the combustion of fossil fuels [1]. However, with increasing energy demands, a finite supply of fossil fuels and growing concern about global warming, there is much interest in long-term, sustainable, and cost-effective alternative energy sources and carriers.

An alternative energy carrier which shows great potential is hydrogen. The benefits of using hydrogen over more conventional fuels include its elemental abundance, high energy content and potential for zero greenhouse gas emissions, with water the only by-product from direct combustion [2,3]. While hydrogen can be produced from a range of sources, including fossil fuels and biomass, one of the simpler methods of production involves the splitting of water [4]. By utilising this process, hydrogen could potentially provide a method for the storage and transport of energy from intermittent sources, such as wind or solar energy, a strategy which would provide flexibility in the utilisation of these renewable energy sources [5]. During the electrolysis of water, hydrogen is produced by the hydrogen evolution reaction (HER, Eq. (1)):

$$2H^+ + 2e^- \rightarrow H_2 \quad (1)$$

Currently the preferred catalysts for the HER are platinum-based catalysts, which are capable of catalysing the HER at overpotentials close to zero [4,5]. However, the scarcity and high material cost of platinum makes it unfeasible for widespread industrial application, as there are insufficient platinum reserves to sustain a substantial large-scale hydrogen producing industry [4]. Over the last few decades, much research has focused on the development and improvement of HER catalysts based around cheaper and more abundant metals, such as the first row transition metals.

However, several efficient HER catalyst already exist in nature. These are members of a class of metalloenzymes called hydrogenases [6]. These enzymes are found in a range of microorganisms, including bacteria and archaea, and are capable of reversibly catalysing the HER at overpotentials that rival those of the platinum-based catalysts [6–8]. There are three types of hydrogenases, which are classed, based on the structure of their active sites, the [NiFe]-, [FeFe]- and [Fe]-hydrogenases, with active sites illustrated in Fig. 1 [8,9]. These three classes have been shown to be evolutionarily unrelated, though they possess some analogous features within their respective active sites [10,11]. The three forms of hydrogenase contain either a mononuclear or a dinuclear

* Corresponding author.
*E-mail address:* thomas.maschmeyer@sydney.edu.au (T. Maschmeyer).

http://dx.doi.org/10.1016/j.apcatb.2017.04.053
0926-3373/

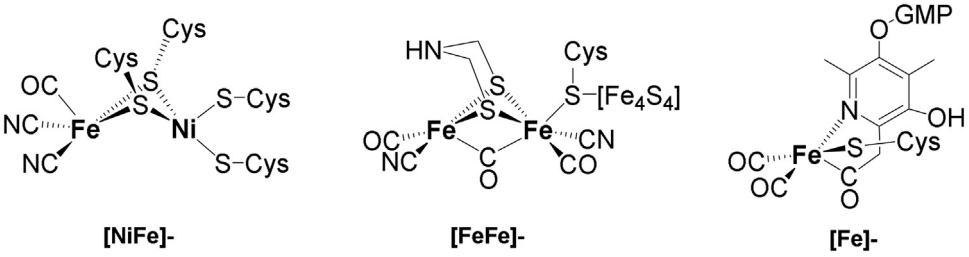


**Fig. 1.** Active sites of the [NiFe]-, [FeFe]- and [Fe]-hydrogenases [8,9].

redox-active metal centre, as well as cyanide and/or carbonyl ligands bound to the metal centre [12]. These ligands are thought to be important in tuning the reactivity of the metal centres, with the arrangement around the metal centre allowing for good overlap between the $\pi^*$-orbitals of the ligands and the filled metal *d*-orbitals stabilising the metal centre, so enabling hydrogen activation [12–14]. The primary interest in these hydrogenases is the inclusion in the active site of iron and nickel, which are relatively abundant and inexpensive first row transition metals.

Much research has focussed on mimicking the active site of the hydrogenase enzymes in the effort to design an efficient and stable catalyst from the abundant first row transition metals [6,15]. One hydrogenase mimic that is capable of catalysing the HER is the $[CpFe(CO)_2(THF)](BF_4)$ (Cp = cyclopentadienyl anion) complex and its analogues [16]. However, one of the major drawbacks of this catalyst is its rapid deactivation, through the dimerisation of the catalytically active species, which results in a low turnover number (TON) of 2 [16]. In addition, the reduction of this complex to the active catalytic species, $[CpFe(CO)_2]^-$, has been reported to occur at −0.80 V *vs* Ag/AgCl in DMF, which corresponds to a relatively large overpotential and, hence, low catalytic efficiency [16].

Different approaches by which the catalytic efficiency of these hydrogenase mimics could be improved include the use of bulky ligands to hinder dimerisation, the addition of more electron withdrawing groups to reduce the overpotential, and the addition of functional groups to link the complex to a solid support to inhibit dimerisation. This paper will focus on exploring the first two approaches and the identification of a possible route to the third. One way to increase the steric bulk around the metal centre could be through the use of a pentaphenylcyclopentadienyl ($Cp^{**}$) ligand. These ligands have previously been reported to improve the kinetic stability of organometallic complexes through their additional steric bulk when compared to the Cp ligand [17]. Furthermore, the $Cp^{**}$ ligand is known to be more electron withdrawing than the Cp ligand, a difference which has been shown to result in a positive shift in the reduction potentials of $Cp^{**}$ palladium complexes [17]. For the catalytic generation of hydrogen this would correspond to a decrease in the overpotential and an increase in catalytic efficiency. The presence of the phenyl groups on the $Cp^{**}$ ligand allows for additional tuning of the catalytic properties by further substitution of these phenyl rings. This paper presents the synthesis and electrochemical study of two related HER catalyst precursors; $[Cp^{**}Fe(CO)_2Br]$ and $[Fe(C_5(p\text{-}C_6H_4Br)_5)(CO)_2Br]$.

## 2. Experimental

### 2.1. Materials

Unless stated otherwise all chemicals were used as received. Tetrahydrofuran (THF) and toluene were dried by passage through a column of activated alumina under 10 bar of nitrogen pressure; in addition the THF was distilled under nitrogen before use. The supporting electrolyte, tetrabutylammonium hexafluorophosphate ($TBAPF_6$, 98%) (Fluka), was recrystallised from ethanol and water before drying under vacuum at 80 °C for a minimum of 12 h. Trichloroacetic acid (Merck) was recrystallised from chloroform and dried over diphosphorus pentoxide (Merck) under vacuum at room temperature.

### 2.2. Synthesis

Tetraphenylcyclopentadienone was synthesised following a procedure by Johnson and Grummit [18]. 1,2,3,4,5-Pentaphenylcyclopentadien-1-ol was synthesised using a method adapted from Field et al. [19] The diethyl ether solvent was substituted with THF and the formation of the Grignard was initiated using a heat gun at 100 °C before further heating the solution for 30 min at 70 °C. 1-Bromo-1,2,3,4,5-pentaphenylcyclopentadiene was synthesised following a method derived from Field et al. [19] 1-Bromo-1,2,3,4,5-penta(*p*-bromophenyl)cyclopentadiene was synthesised following a procedure adapted from Carella et al. [20]

The two iron complexes $[Cp^{**}Fe(CO)_2Br]$ and $[Fe(C_5(p\text{-}C_6H_4Br)_5)(CO)_2Br]$ were synthesised from their respective ligand precursors using a method adapted from McVey and Pauson, with benzene replaced by toluene as the solvent [21]. $[Cp^{**}Fe(CO)_2Br]$ was recrystallised from dichloromethane and hexane rapidly using a rotary evaporator, while $[Fe(C_5(p\text{-}C_6H_4Br)_5)(CO)_2Br]$ was recrystallised from dichloromethane and hexane at −20 °C.

**$[Fe(C_5(p\text{-}C_6H_4Br)_5)(CO)_2Br]$ data:** dark red crystals, decomposed without melting. **$^1$H NMR** (300 MHz, $CDCl_3$): $\delta$ 6.9 (10H, d, $^3J_{HH}$ = 8.4 Hz, ArH), 7.3 (10H, d, $^3J_{HH}$ = 8.1 Hz, ArH) ppm. **$^{13}$C[$^1$H] NMR** (75 MHz, $CDCl_3$): $\delta$ 99.9, 123.6, 128.0, 131.6, 133.5 ppm. **Selected APCI-MS data** *m*/*z* (%): 841 (29), 762 (13), 705 (21), 689 (100). **Selected IR data (neat)**: 3043 ($\nu$CH; w, b), 2034 ($\nu$CO; s), 1994 ($\nu$CO; s), 1655 (m), 1587 (w), 1493 (m), 1431 (w), 1385 (m), 1264 (w), 1182 (w), 1070 (s), 1009 (s), 825 (s), 770 (s), 751 (m) $cm^{-1}$. **Anal. Calc. for $C_{37}H_{20}Br_6FeO_2$:** C, 43.07; H, 1.95. **Found:** C, 42.53; H, 2.17.

### 2.3. Characterisation

A single crystal X-ray diffraction structural analysis for $[Fe(C_5(p\text{-}C_6H_4Br)_5)(CO)_2Br]$ was performed by using an Agilent SuperNova Dual diffractometer equipped with an Atlas detector and employing mirror monochromated Cu (Kα) radiation from a micro-source. Cell constants were obtained from least squares refinement against 47017 reflections located between 6 and 152° 2θ. Data were collected at 150(1) Kelvin with ω scans to 152° 2θ. The data processing was undertaken with CrysAlis Pro[22] and subsequent computations were carried out using the WinGX[23] and ShelXle interfaces [24]. A multi-scan absorption correction was applied to the data [22]. The structure was solved by direct methods with SHELXT[25] and extended and refined with SHELXL-2014/7 [26]. An ORTEP depiction with 50% displacement ellipsoids is provided in Fig. 2 [27,28]. Details for the structural characterisation for both $[Cp^{**}Fe(CO)_2(FBF_3)]$ and $[Cp^{**}Fe(CO)_2(OH_2)](BF_4)$ can be found in the ESI. The data for the three complexes have been deposited with

the Cambridge Crystallographic Data Centre as CCDC 1509846-1509848.

The asymmetric unit contains a complex molecule together with a dichloromethane solvate molecule. Residual electron density indicated the bromido and one carbonyl ligand were disordered over two sites and complementary occupancies were refined and then fixed at 0.9 and 0.1 respectively. Distance restraints were required for the minor occupancy carbonyl sites. In general, non-hydrogen atom sites were modelled with anisotropic displacement parameters. Isotropic displacement parameters were assigned and fixed for the minor occupancy carbonyl atoms of the model. A riding atom model with group displacement parameters were used for the hydrogen atoms. (See ESI for crystal data†)

### 2.4. Electrochemistry

All electrochemical measurements were completed in anhydrous DMF under argon at room temperature using an eDAQ ER466 Integrated Potentiostat System.

For cyclic voltammetry a standard three electrode cell configuration was used. The working, counter and pseudo-reference electrodes were as follows: glassy carbon electrode (1.6 mm), a platinum coated tungsten electrode and a leakless Ag/AgCl electrode (3.4 M KCl, eDAQ). A 2.5 mL cell with stirrer bar and lid for multiple electrodes was used. The glassy carbon working electrode was polished with alumina powder (0.3 μm, SLS Lapidary), before use and between runs, on a Buehler polishing micro-pad followed by rinsing with de-ionised water and acetone. The leakless Ag/AgCl pseudo-reference electrode was stored in de-ionised water before use and was washed with de-ionised water and acetone between runs. The platinum coated counter electrode was rinsed with de-ionised water and acetone between runs.

A solution of tetrabutylammonium hexafluorophosphate ($TBAPF_6$, 0.1 M) in DMF was used as the electrolyte. Unless stated otherwise the concentration of the iron complex used was 1 mM. Before each run the sample was deoxygenated by bubbling argon through the solution for 5 min. During each experiment a background scan of the electrolyte was completed before the experiment and a ferrocene calibration was completed after sample testing, all measurements are reported *vs* $Fc^{0/+}$ (which, in the present work, occurs at +0.445 V *vs* Ag/AgCl in DMF) [29].

Controlled potential electrolysis measurements were completed using a set-up described by Bond [30]. The working, counter and pseudo-reference electrodes were as follows: glassy carbon electrode (15.5 $cm^2$), a platinum wire electrode and a leakless Ag/AgCl electrode (3.4 M KCl, eDAQ). The current passed by a 5 mL solution of the iron complex (1 mM) was measured at −1.0 V, in the presence of trichloroacetic acid (1 M) and $TBAPF_6$ (0.1 M) in DMF.

### 2.5. Computational methods

All DFT calculations were performed using Gaussian 09 [31]. Geometries and vibrational frequencies were obtained at the PBE/LanL2MB level. Unscaled PBE/LanL2MB harmonic vibrational frequencies were used to obtain the zero-point vibrational energies and thermal corrections for enthalpies and entropies at 298 K for the fully optimized structures unscaled PBE/LanL2MB harmonic vibrational frequencies were used. Refined single-point energies were obtained at the M06-2X/maug-cc-pVTZ level [32], with the effect of solvation incorporated using the SMD model[33] in conjunction with parameters for DMF.

## 3. Results and discussion

### 3.1. Synthesis and structural characterisation

The synthesis and molecular structure of the $[Cp^{**}Fe(CO)_2Br]$ complex has been reported previously [21,34]. The $[Fe(C_5(p\text{-}C_6H_4Br)_5)(CO)_2Br]$ complex was successfully synthesised using a similar method and its molecular structure confirmed by X-ray crystallographic analysis (Fig. 2). Residual electron density indicated the bromido and one carbonyl ligand were disordered over two sites, and complementary occupancies were refined and then fixed at 0.9 and 0.1 respectively.

It is important to note that while both $[Cp^{**}Fe(CO)_2Br]$ and $[Fe(C_5(p\text{-}C_6H_4Br)_5)(CO)_2Br]$ possess a bromido ligand, the

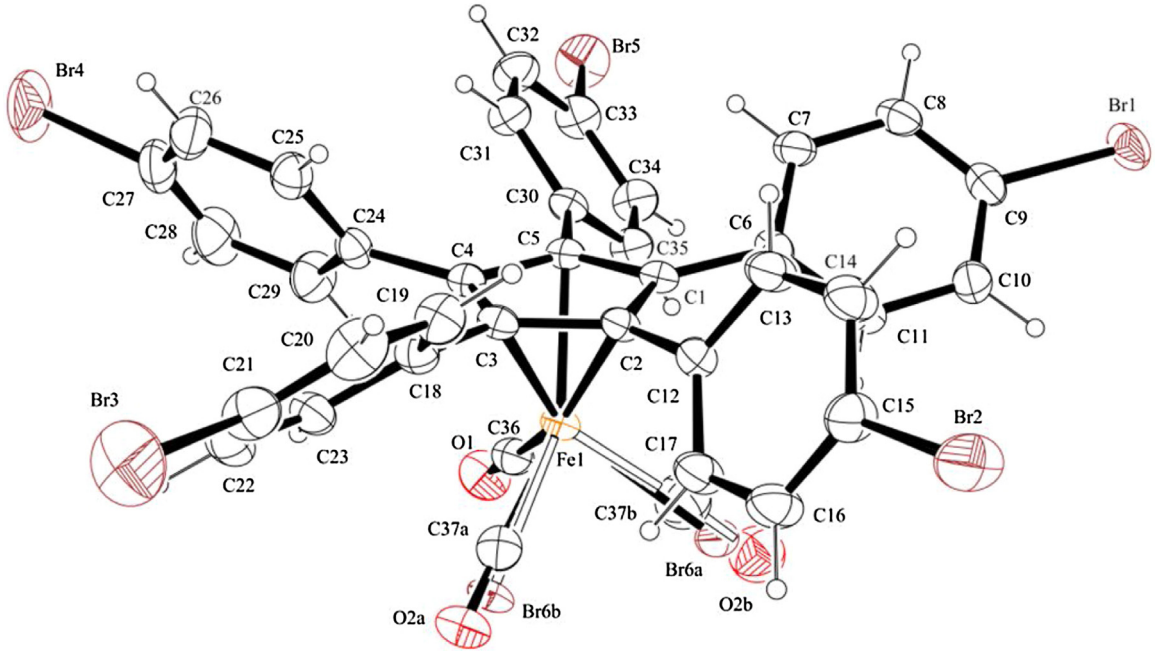


**Fig. 2.** ORTEP depiction the single crystal X-ray diffraction structure of $[Fe(C_5(p\text{-}C_6H_4Br)_5)(CO)_2Br]$, showing 50% displacement ellipsoids and the atomic scheme. The structure's dichloromethane solvate molecule is not shown.

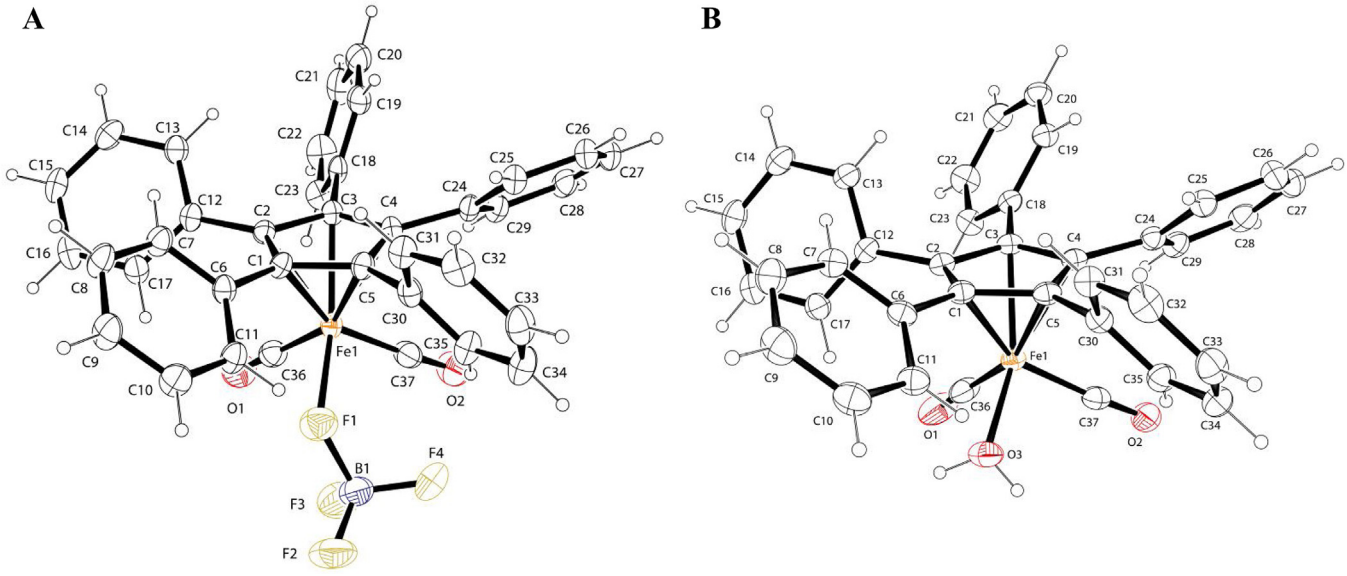


**Fig. 3.** ORTEP depictions of the single crystal X-ray diffraction structure of (A) the $[Cp^{**}Fe(CO)_2(FBF_3)]$ complex molecule and (B) the $[Cp^{**}Fe(CO)_2(OH_2)]^+$ complex cation. Solvate molecules and the $BF_4^-$ counterion for the aqua complex are not shown. Displacement ellipsoids are shown at the 50% level.

lability of this ligand is crucial to the catalytic activity of these complexes. The lability of the bromido ligand of $[Cp^{**}Fe(CO)_2Br]$, was confirmed by reacting it with $AgBF_4$ to produce $[Cp^{**}Fe(CO)_2(FBF_3)]$. The halide extraction by $AgBF_4$ was first observed for the analogous $[CpFe(CO)_2I]$ complex [35]. Like the previously reported $[CpFe(CO)_2(FBF_3)]$ complex, $[Cp^{**}Fe(CO)_2(FBF_3)]$ was found to be hydroscopic, slowly reacting with water to produce $[Cp^{**}Fe(CO)_2(OH_2)](BF_4)$. The molecular structures of these two complexes were confirmed by X-ray crystallography (Fig. 3). The synthesis methods and crystallographic data for both $[Cp^{**}Fe(CO)_2(FBF_3)]$ and $[Cp^{**}Fe(CO)_2(OH_2)](BF_4)$ can be found in the supplementary data. A labile ligand is essential to the catalytic activity of these complexes with the loss of the labile ligand providing a vacant metal centre site to which a proton can bind, enabling hydrogen generation. As shown in the next section, the bromido ligand is labile enough to enable catalytic reactivity *in situ* without the need to form the more labile $[Fe(C_5Ar_5)(CO)_2(FBF_3)]$ complexes.

### 3.2. Cyclic voltammetry

The catalytic efficiencies of $[Cp^{**}Fe(CO)_2Br]$ and $[Fe(C_5(p\text{-}C_6H_4Br)_5)(CO)_2Br]$ were studied and compared using electrochemistry techniques, including cyclic voltammetry and controlled potential electrolysis. The cyclic voltammogram of $[Cp^{**}Fe(CO)_2Br]$ in DMF (Fig. 4) contains a single reductive peak with a half-wave potential ($E_{1/2}$) of −1.13 V *vs* $Fc^{0/+}$. This process was identified as a two electron reduction of the complex, by comparison of current maxima with a standard ferrocene solution. The overall electrode process results in the formation of $[Cp^{**}Fe(CO)_2]-$ *via* an electrochemical chemical electrochemical (ECE) mechanism, which has been previously described for the $[CpFe(CO)_2I]$ complex [36]. The proposed mechanism is shown below (Eqs. (2)–(4)). The intermediate, $[Cp^{**}Fe(CO)_2]$, is produced at a potential more negative than its reduction and so is reduced upon generation.

$$[Cp^{**}Fe^{II}(CO)_2Br] + e^- \rightleftharpoons [Cp^{**}Fe^{I}(CO)_2Br]^- \quad (2)$$

$$[Cp^{**}Fe^{I}(CO)_2Br]^- \rightarrow [Cp^{**}Fe^{I}(CO)_2] + Br^- \quad (3)$$

$$[Cp^{**}Fe^{I}(CO)_2] + e^- \rightleftharpoons [Cp^{**}Fe^{0}(CO)_2]^- \quad (4)$$

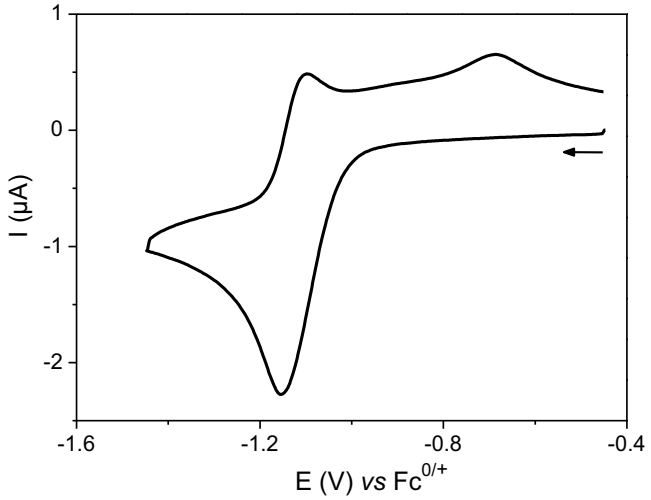


**Fig. 4.** Cyclic voltammogram of $[Cp^{**}Fe(CO)_2Br]$ (1 mM) *vs* $Fc^{0/+}$, in 0.1 M $TBAPF_6$ in DMF at a scan rate of 100 mV $s^{-1}$ (Initial potential −0.445 V *vs* $Fc^{0/+}$).

This process is not reversible, as shown by a cathodic to anodic peak current ratio ($I_{pc}/I_{pa}$) of 2.25, suggesting that the reduction involves twice as many electrons as the re-oxidation of the reduced species. The irreversibility of this process can be ascribed to the irreversibility of the chemical reaction in Eq. (3) [36].

A similar ECE reductive process was also observed for the $[Fe(C_5(p\text{-}C_6H_4Br)_5)(CO)_2Br]$ complex in DMF (Fig. 5), which occurred with a $E_{1/2}$ of −0.99 V *vs* $Fc^{0/+}$. This process is shifted to a more positive potential by around 140 mV compared to that of $[Cp^{**}Fe(CO)_2Br]$. However, a minor irreversible peak was also observed at −0.89 V during the first scan of the complex. The ratio of the peak currents of these two reductive peaks could be shifted by the incremental addition of bromide, as $Bu_4NBr$ (Fig. S1†), with an increase in the relative peak current of the minor peak at −0.89 V. This suggests that the two reductive processes may be due to an equilibrium between the non-solvated and the solvated complex respectively (Eq. (5)), with the addition of bromide ions shifting the equilibrium to favour the formation of the non-solvated complex:

$$[\{C_5(p\text{-}C_6H_4Br)\}Fe^{II}(CO)_2Br] + DMF \rightleftharpoons [\{C_5(p\text{-}C_6H_4Br)\}Fe^{II}(CO)_2(DMF)]^+ + Br^- \quad (5)$$

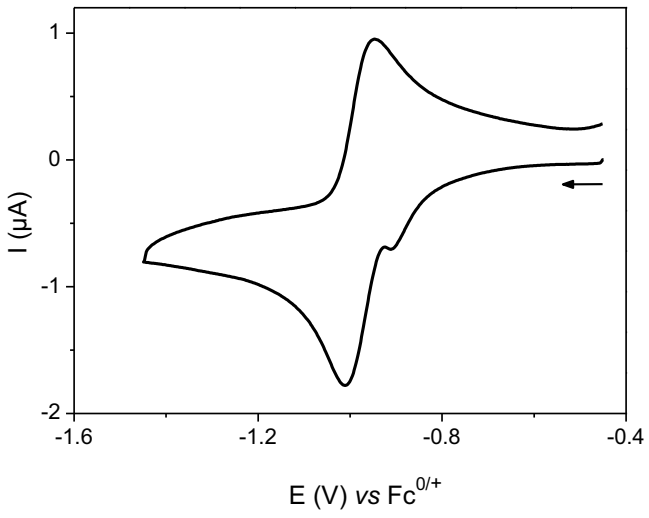


**Fig. 5.** Cyclic voltammogram of $[Fe(C_5(p\text{-}C_6H_4Br)_5)(CO)_2Br]$ (1 mM) *vs* $Fc^{0/+}$, in 0.1 M $TBAPF_6$ in DMF at a scan rate of 100 mV $s^{-1}$ (Initial potential −0.445 V *vs* $Fc^{0/+}$).

The increase in current of the minor peak with increasing bromide concentration suggests that this peak is due to the reduction of the non-solvated complex and, hence, the major peak must be due to the reduction of the solvated complex. The solvated complex is more difficult to reduce as indicated by the slightly more negative reduction potential, which may be due to the higher concentration of DMF making the loss of the solvated molecule less favourable than the loss of the bromido ligand.

While the $E_{1/2}$ for formation of the catalytically active species for $[Fe(C_5(p\text{-}C_6H_4Br)_5)(CO)_2Br]$ occurs at a more positive potential than for $[Cp^{**}Fe(CO)_2Br]$, the reduction of both of these complexes occurs at more positive potentials than $[CpFe(CO)_2(THF)](BF_4)$, which forms the active catalytic species at −1.33 V *vs* $Fc^{0/+}$ (−0.80 V *vs* Ag/AgCl) [16]. The catalytically active species is formed by the reduction of the metal centre to the electron rich $Fe^0$ species. The $Cp^{**}$ ligand is known to be more electron withdrawing than then Cp ligand [17,34]. This electron withdrawal from the metal centre is expected to stabilise the catalytically active species of $[Cp^{**}Fe(CO)_2(solv)]^+$ more than $[CpFe(CO)_2(THF)](BF_4)$, favouring the reduction of the $Cp^{**}$ derivative, as observed by the shift in the reduction potential. The enhanced shift of the formally $Fe^{II}$ to $Fe^0$ reduction of $[Fe(C_5(p\text{-}C_6H_4Br)_5)(CO)_2Br]$ from that of $[CpFe(CO)_2(THF)](BF_4)$ is, therefore, likely caused by the additional electron withdrawing effects of the substituent bromide atoms. We discuss this hypothesis more fully in the following paragraph.

If the substituents are affecting the electron density of the metal centre, then it is reasonable to expect a correlation between the electron donating/withdrawing effect of the substituent and the $E_{1/2}$. Plotting the relative Hammett substituent constant, a measure of the electron donating/withdrawing effect, against the $E_{1/2}$ for three different substituted iron complexes did show some linearity (Fig. S2†). This suggests a correlation between the shift in the $E_{1/2}$ observed and the electron withdrawing effect of the substituent bromide atoms. A more in-depth discussion of this can be found in the supplementary data. Furthermore, analysis of the two iron complexes by IR spectroscopy additionally confirmed the capacity of the substituents to influence the electron density of the metal centre. The two peaks which can be attributed to the symmetric and anti-symmetric carbonyl stretches were found to shift to higher frequencies with the addition of the substituents, from 2027 and 1984 $cm^{-1}$ for $[Cp^{**}Fe(CO)_2Br]$ to 2034 and 1994 $cm^{-1}$ for $[Fe(C_5(p\text{-}C_6H_4Br)_5)(CO)_2Br]$. This change in frequency indicates that the presence of the p-bromide substituents on the $Cp^{**}$ ligand withdraws electron density from the iron centre. This results in a lower electron density on the iron, available for back-donation into the $\pi^*$-antibonding orbitals of the carbonyls compared to $[Cp^{**}Fe(CO)_2Br]$, leading to stronger C—O bonds and, hence, the observed increase in the frequency of the carbonyl stretches.

Of importance to note is that during the timeframe for the cyclic voltammetry experiments, no colour change or precipitate formation was observed for either of the complexes. Additionally, multiple scans of the same solution showed negligible differences in the voltammograms. The lack of any observable colour change or precipitate and no reduction in the peak current suggests the lack of any material from the decomposed catalyst covering the electrode [37].

### 3.3. Electrocatalytic hydrogen evolution

Increasing the concentration of trichloroacetic acid (TCA) in a solution of $[Cp^{**}Fe(CO)_2Br]$ or $[Fe(C_5(p\text{-}C_6H_4Br)_5)(CO)_2Br]$ in DMF led to the formation of a catalytic wave (Fig. 6), attributable to the catalytic generation of hydrogen. The overpotential, TON and kinetics for the two catalysts were measured in order to give a measure

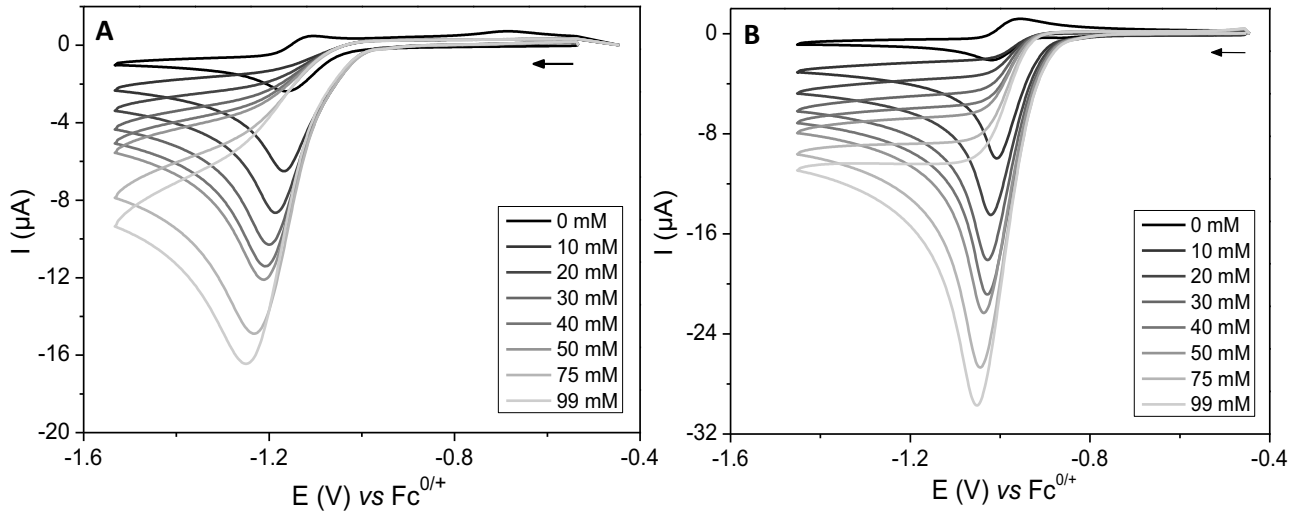


**Fig. 6.** Cyclic voltammograms of $[Cp^{**}Fe(CO)_2Br]$ (**A**) and $[Fe(C_5(p\text{-}C_6H_4Br)_5)(CO)_2Br]$ (B) *vs* $Fc^{0/+}$ with the addition of trichloroacetic acid (0–99 mM), in 0.1 M $TBAPF_6$ in DMF at a scan rate of 100 mV $s^{-1}$ (Initial potential −0.445 V *vs* $Fc^{0/+}$).

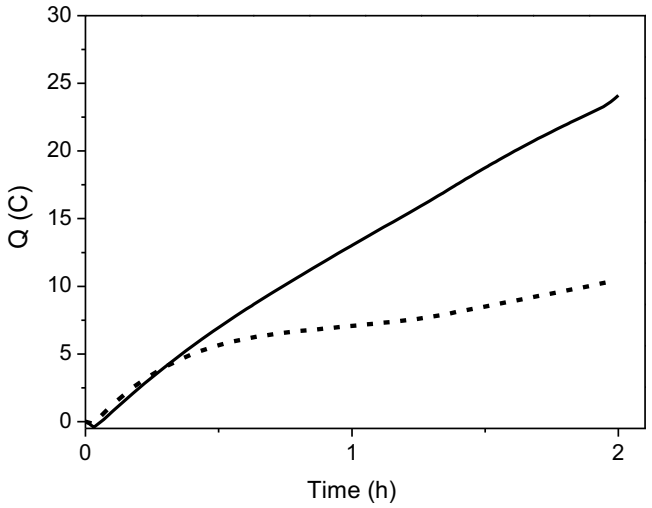


**Fig. 7.** Coulometry for bulk electrolysis at −1.0 V *vs* Ag/AgCl of a DMF solution (5 mL) of trichloroacetic acid (1 M) and $TBAPF_6$ (0.1 M) at a glassy carbon electrode in the presence of 1 mM of [Cp**Fe(CO)$_2$Br] (dashed) or [Fe(C$_5$(*p*-C$_6$H$_4$Br)$_5$)(CO)$_2$Br] (solid).

of their efficiency as HER catalysts. The overpotential for catalysts was measured by calculating the difference between the standard reduction potential for hydrogen ($E_{H^+}$) and the catalytic half-wave potential ($E_{cat/2}$) which is the potential at half the current of the catalytic wave (Eq. (6)) [38]:

$$Overpotential = |E_{H^+} - E_{cat/2}| \quad (6)$$

The overpotentials for these complexes were estimated assuming a standard reduction potential for hydrogen of −0.642 V *vs* $Fc^{0/+}$ (−0.197 V *vs* Ag/AgCl) [29]. At a 10 mM concentration of TCA the overpotentials for [Cp**Fe(CO)$_2$Br] and [Fe(C$_5$(*p*-C$_6$H$_4$Br)$_5$)(CO)$_2$Br] were approximately 450 mV and 310 mV, respectively. The additional electron withdrawing effects of the C$_5$(*p*-C$_6$H$_4$Br)$_5$ ligand improves the catalytic efficiency by causing a 140 mV decrease of the overpotential for this catalyst.

Controlled potential electrolysis was used to establish the TONs for the two complexes and to give a measure of their stability. The TON for [Cp**Fe(CO)$_2$Br] and [Fe(C$_5$(*p*-C$_6$H$_4$Br)$_5$)(CO)$_2$Br] were calculated from the total current (Q) passed by the complexes after 2 h at −1.00 V *vs* Ag/AgCl in a solution of TCA (1 M) in DMF, and were found to be 11 and 25 respectively (Fig. 7). While neither of these complexes complete a large number of turnovers in the time of the experiment, both undergo significantly more turnovers than reported for [CpFe(CO)$_2$(THF)](BF$_4$), which has a TON of 2, with [Fe(C$_5$(*p*-C$_6$H$_4$Br)$_5$)(CO)$_2$Br] completing over twice as many turnovers as [Cp**Fe(CO)$_2$Br] [16]. This may be due to both the stabilisation of the Fe(0) catalytic species through the increasingly electron withdrawing ligands and the additional steric bulk provided by the ligands, both of which should inhibit the dimerisation of the complex. Using cyclic voltammetry to scan the solutions used for the controlled potential electrolysis showed the complete loss of the reductive peaks and a change in the colour of the solution for both complexes after 2 h. This confirmed the decomposition of the complexes.

The kinetics for catalysis of the HER for the complexes were determined by plotting the concentration of TCA against the ratio of the catalytic current ($I_c$) and the peak current in the absence of acid for the two catalysts ($I_p$) from Fig. 6 (Fig. S3†) [39]. At low concentrations of TCA there is a linear relationship between acid concentration and the $I_c/I_p$, indicating a second-order dependence of the catalytic cycle on the acid concentration (Fig. S4†) [40]. As the concentration of TCA increases, the catalyst reaches a maximum turnover rate, obeying Michaelis–Menten kinetics, as shown by the plateau in the graph which signifies a zero-order dependence on the acid concentration (Fig. S3†) [39]. Similarly, plotting the concentration of both complexes against $I_c$, a linear plot is obtained (Fig. S5†), indicating a first-order dependence on the catalyst concentration.

**Table 1**
Calculated rate constants for [Cp**Fe(CO)$_2$Br] and [Fe(C$_5$(*p*-C$_6$H$_4$Br)$_5$)(CO)$_2$Br] at low ($k_{obs}$) and high ($k_{constant}$) concentrations of trichloroacetic acid.

| | [Cp**Fe(CO)$_2$Br] | [Fe(C$_5$(p-C$_6$H$_4$Br)$_5$)(CO)$_2$Br] |
|---|---|---|
| $k_{obs}$ ($M^{-2}\,s^{-1}$) | 624 ± 61 | 2417 ± 206 |
| $k_{constant}$ ($s^{-1}$) | 148 ± 5 | 533 ± 15 |

At low concentrations of acid, the rate constant ($k_{obs}$) can be calculated using Eq. (7), where R is the gas constant, T is the temperature in Kelvin, F is Faraday's constant, $\nu$ is the scan rate and $n$ is the number of electrons consumed in the reaction (n = 2 for hydrogen production) [40].

$$\frac{I_c}{I_p} = \frac{n}{0.4463} \times \sqrt{\frac{RT}{F}\left(\frac{k_{obs}[H^+]^2}{\nu}\right)} \quad (7)$$

When the rate of reaction is independent of the acid concentration, the rate constant ($k_{constant}$) can be calculated using Eq. (8), where $n$' is the number electrons involved in the reduction of the complex in the absence of acid [39].

$$\langle removepicturepageno10\rangle \frac{I_c}{I_p} = \frac{n}{0.4463(n')^{3/2}} \times \sqrt{\frac{RT \times k_{constant}}{F\nu}} \quad (8)$$

Using these two equations, the rate constants at high and low concentration of acid were calculated for both complexes (Table 1). This analysis indicates that [Fe(C$_5$(*p*-C$_6$H$_4$Br)$_5$)(CO)$_2$Br] catalyses the HER over 3.5 times faster than [Cp**Fe(CO)$_2$Br], which was unexpected. The more electron withdrawing C$_5$(*p*-C$_6$H$_4$Br)$_5$ ligand was expected to reduce the electron density of the catalytically active Fe(0) species, making it harder to protonate and resulting in slower reaction rates.

### 3.4. Computational modelling

Computational modelling was used in order to investigate the reason for the difference in the rates of reaction for [Cp**Fe(CO)$_2$Br] and [Fe(C$_5$(*p*-C$_6$H$_4$Br)$_5$)(CO)$_2$Br]. This was completed by calculating the ΔG values for each step of the catalytic cycle for these complexes. Two different catalytic mechanisms have been proposed for the analogous [CpFe(CO)$_2$(THF)](BF$_4$) and [CpFe(CO)$_2$H] complexes [16,41]. While these two catalytic cycles are similar, the main distinction between the two cycles is the occurrence of the second reduction of the metal centre, with Artero and Fontecave suggesting that this step occurs after the formation of $H_2$, while Felton et al. suggest this occurs before the formation of $H_2$ [16,41].

DFT calculations were used to predict ΔG values, at 298 K in the gaseous phase, for the different steps of a catalytic cycle (Fig. 8) proposed for [CpFe(CO)$_2$(THF)](BF$_4$) [16]. While the simplicity of the model computations does not offer a quantitative comparison with the experimental data, the predicted ΔG values for most of these steps are qualitatively more favourable for [Fe(C$_5$(*p*-C$_6$H$_4$Br)$_5$)(CO)$_2$Br]. This is consistent with the increased ability of the *p*–bromophenyl moieties to stabilise the iron centre by reducing the density of electrons around this metal centre facilitating its reduction, compared to the complex with unsubstituted phenyl rings [17]. This additional stabilisation could account for the faster rate of reaction observed for [Fe(C$_5$(*p*-C$_6$H$_4$Br)$_5$)(CO)$_2$Br]. The calculations also show that the protonation of the Fe(0) species and the subsequent generation of hydrogen is slightly more energetically favourable for [Fe(C$_5$(*p*-C$_6$H$_4$Br)$_5$)(CO)$_2$Br] than for

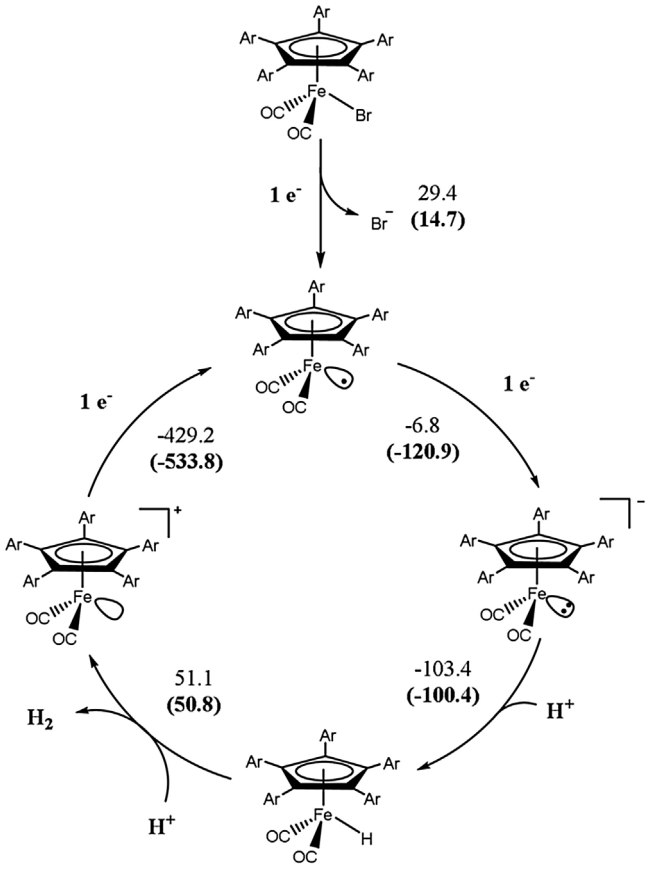


**Fig. 8.** DFT predictions of the Gibbs free energy (kJ mol$^{-1}$), showing values for [Cp**Fe(CO)$_2$Br] and in bold [Fe(C$_5$(*p*-C$_6$H$_4$Br)$_5$)(CO)$_2$Br], for each step of the catalytic cycle proposed by Artero and Fontecave [16].

[Cp**Fe(CO)$_2$Br]. Similar results were obtained when the ΔG values were predicted for the steps for the catalytic cycle proposed for [CpFe(CO)$_2$H] (Fig. S6†). The main differences being that all steps except the first were energetically favoured and that the reduction of the [Fe(C$_5$Ar$_5$)(CO)$_2$H] species was slightly more energetically favoured for [Cp**Fe(CO)$_2$Br]. However, the small difference in the ΔG values between the catalysts for this step is likely to have a negligible impact on the rates of reaction. Thus, these *ab initio* computational results rationalise the increased rate constants observed for [Fe(C$_5$(*p*-C$_6$H$_4$Br)$_5$)(CO)$_2$Br].

## 4. Conclusions

The addition of phenyl rings to the Cp ligand was shown to confer steric bulk, which improved the stability of these Fe(II)-based hydrogenase mimics by suppressing the dimerisation of components in the proposed catalytic cycle. The presence of the more electron withdrawing C$_5$(*p*-C$_6$H$_4$Br)$_5$ ligand further stabilised the catalytically active species, leading to a decrease in the overpotential of 140 mV compared to that of the complex with the unsubstituted Cp** ligand. In addition, [Fe(C$_5$(*p*-C$_6$H$_4$Br)$_5$)(CO)$_2$Br] was also found to have the highest TON and the fastest rate of reaction. The presence of the *p*-bromophenyl groups should allow for further substitution with functional groups, which could then be used to bind these complexes to a surface. This could potentially be explored as another method to further improve the stability of these hydrogenase mimics.

The data presented in this paper suggest that the rational design of the substituted Cp** ligand could be utilised as a means to improve these HER catalysts, potentially leading to the development of an efficient and cheap catalyst for the commercially viable and sustainable production of hydrogen.

## Acknowledgements

This work was supported by the Australian Research Council and the Japan Society for the Promotion of Science (16H07074). Data for the structure of [Cp**Fe(CO)$_2$(OH$_2$)](BF$_4$) complex were obtained on the MX1 beamline at the Australian Synchrotron, Victoria, Australia. Computer time for quantum chemistry calculations was provided by RIKEN Advanced Center for Computing and Communication, Japan and Institute for Molecular Science, Japan. We thank Michael Burke, Francois Noverraz and Edar Chan for preliminary experiments.

## Appendix A. Supplementary data

Supplementary data associated with this article can be found, in the online version, at http://dx.doi.org/10.1016/j.apcatb.2017.04.053.

## References

[1] World Energy Investment Outlook, International Energy Agency, France, 2014.
[2] C.M. Kalamaras, A.M. Efstathiou, Conf. Pap. Energy 2013 (2013) 9.
[3] A. Haryanto, S. Fernando, N. Murali, S. Adhikari, Energy Fuels 19 (2005) 2098–2106.
[4] M. Tavakkoli, T. Kallio, O. Reynaud, A.G. Nasibulin, C. Johans, J. Sainio, H. Jiang, E.I. Kauppinen, K. Laasonen, Angew. Chem. Int. Ed. 54 (2015) 4535–4538.
[5] J.R. McKone, S.C. Marinescu, B.S. Brunschwig, J.R. Winkler, H.B. Gray, Chem. Sci. 5 (2014) 865–878.
[6] S. Kaur-Ghumaan, M. Stein, Dalton Trans. 43 (2014) 9392–9405.
[7] D.-H. Kim, M.-S. Kim, Bioresour. Technol. 102 (2011) 8423–8431.
[8] T.R. Simmons, G. Berggren, M. Bacchi, M. Fontecave, V. Artero, Coord. Chem. Rev. 270 (2014) 127–150.
[9] D.M. Heinekey, J. Organomet. Chem. 694 (2009) 2671–2680.
[10] D.W. Mulder, E.M. Shepard, J.E. Meuser, N. Joshi, P.W. King, M.C. Posewitz, J.B. Broderick, J.W. Peters, Structure 19 (2011) 1038–1052.
[11] M.T. Stiebritz, M. Reiher, Inorg. Chem. 49 (2010) 5818–5823.
[12] M.W.W. Adams, E.I. Stiefel, Curr. Opin. Chem. Biol. 4 (2000) 214–220.
[13] L. Forzi, P. Hellwig, R.K. Thauer, R.G. Sawers, FEBS Lett. 581 (2007) 3317–3321.
[14] A.L. De Lacey, V.M. Fernández, M. Rousset, R. Cammack, Chem. Rev. 107 (2007) 4304–4330.
[15] P. Du, R. Eisenberg, Energy Environ. Sci. 5 (2012) 6012–6021.
[16] V. Artero, M. Fontecave, C.R. Chim. 11 (2008) 926–931.
[17] K. Broadley, G.A. Lane, N.G. Connelly, W.E. Geiger, J. Am. Chem. Soc. 105 (1983) 2486–2487.
[18] J.R. Johnson, O. Grummitt, Org. Syn. 23 (1943) 92–93.
[19] L.D. Field, K.M. Ho, C.M. Lindall, A.F. Masters, A.G. Webb, Aust. J. Chem. 43 (1990) 281–291.
[20] A. Carella, J.P. Launay, R. Poteau, G. Rapenne, Chem.—Eur. J. 14 (2008) 8147–8156.
[21] S. McVey, P.L. Pauson, J. Chem. Soc. (1965), 4312-&.
[22] CrysAlisPro Version 1.171.37.35., Agilent Technologies, 2015.
[23] L.J. Farrugia, J. Appl. Crystallogr. 32 (1999) 837–838.
[24] C.B. Huebschle, G.M. Sheldrick, B. Dittrich, J. Appl. Crystallogr. 44 (2011) 1281–1284.
[25] G.M. Sheldrick, Acta Crystallogr.—Found. Adv. 71 (2015) 3–8.
[26] G.M. Sheldrick, Acta Crystallogr. A 64 (2008) 112–122.
[27] L.J. Farrugia, J. Appl. Crystallogr. 30 (1997) 565.
[28] M.N. Burnett, C.K. Johnson, ORTEP III, ORTEP-III Report ORNL-6895, Oak Ridge National Laboratory, Tennessee, USA, 1996.
[29] P. Zanello, Inorganic Electrochemistry: Theory, Practice and Application, The Royal Society of Chemistry, Cambridge, 2003.
[30] A.M. Bond, Broadening Electrochemical Horizons: Principles and Illustration of Voltammetric and Related Techniques, Oxford University Press, Oxford, 2002.
[31] Gaussian 09, Revision C.01, M.J. Frisch, G.W. Trucks, H.B. Schlegel, G.E. Scuseria, M.A. Robb, J.R. Cheeseman, G. Scalmani, V. Barone, B. Mennucci, G.A. Petersson, H. Nakatsuji, M. Caricato, X. Li, H.P. Hratchian, A.F. Izmaylov, J. Bloino, G. Zheng, J.L. Sonnenberg, M. Hada, M. Ehara, K. Toyota, R. Fukuda, J. Hasegawa, M. Ishida, T. Nakajima, Y. Honda, O. Kitao, H. Nakai, T. Vreven, J.A. Montgomery, Jr., J.E. Peralta, F. Ogliaro, M. Bearpark, J.J. Heyd, E. Brothers, K.N. Kudin, V.N. Staroverov, R. Kobayashi, J. Normand, K. Raghavachari, A. Rendell, J.C. Burant, S.S. Iyengar, J. Tomasi, M. Cossi, N. Rega, J.M. Millam, M. Klene, J.E. Knox, J.B. Cross, V. Bakken, C. Adamo, J. Jaramillo, R. Gomperts, R.E. Stratmann, O. Yazyev, A.J. Austin, R. Cammi, C. Pomelli, J.W. Ochterski, R.L. Martin, K. Morokuma, V.G. Zakrzewski, G.A. Voth, P. Salvador, J.J. Dannenberg, S.

Dapprich, A.D. Daniels, Ö.F. Farkas, J.B., J.V. Ortiz, J. Cioslowski, D.J. Fox, Gaussian, Inc., Wallingford CT, 2016.
[32] Y. Zhao, D.G. Truhlar, Theor. Chem. Acc. 120 (2008) 215–241.
[33] A.V. Marenich, C.J. Cramer, D.G. Truhlar, J. Phys. Chem. B 113 (2009) 6378–6396.
[34] L.D. Field, T.W. Hambley, C.M. Lindall, A.F. Masters, Polyhedron 8 (1989) 2425–2430.
[35] B.M. Mattson, W.A.G. Graham, Inorg. Chem. 20 (1981) 3186–3189.
[36] T. Munisamy, S.L. Gipson, J. Organomet. Chem. 692 (2007) 1087–1091.
[37] E.S. Donovan, G.A.N. Felton, J. Organomet. Chem. 711 (2012) 25–34.
[38] A.M. Appel, M.L. Helm, ACS Catal. 4 (2014) 630–633.
[39] D.H. Pool, D.L. DuBois, J. Organomet. Chem. 694 (2009) 2858–2865.
[40] A.D. Wilson, R.H. Newell, M.J. McNevin, J.T. Muckerman, M. Rakowski DuBois, D.L. DuBois, J. Am. Chem. Soc. 128 (2006) 358–366.
[41] G.A.N. Felton, A.K. Vannucci, N. Okumura, L.T. Lockett, D.H. Evans, R.S. Glass, D.L. Lichtenberger, Organometallics 27 (2008) 4671–4679.